CrystEngComm

Hierarchical Spheres of Mg-Al LDH for Removal of Phosphate Ions: Effect of Alumina Polymorph as Precursor

Journal:	*CrystEngComm*
Manuscript ID	CE-ART-07-2019-001064.R1
Article Type:	Paper
Date Submitted by the Author:	24-Sep-2019
Complete List of Authors:	Sudare, Tomohito; Shinshu University Zenzai, Atsushi; Shinshu University Tamura, Shuhei; Shinshu University Kiyama, Masahiro; Shinshu University Hayashi, Fumitaka; Shinshu University, Faculty of Engineering Teshima, Katsuya; Shinshu University, Department of Materials Chemistry; Shinshu University, Center for Energy and Environmental Science

Journal Name

ARTICLE

Hierarchical Spheres of Mg-Al LDH for Removal of Phosphate Ions: Effect of Alumina Polymorph as Precursor

Received 00th January 20xx,
Accepted 00th January 20xx

DOI: 10.1039/x0xx00000x

www.rsc.org/

Tomohito Sudare,[a] Atsushi Zenzai,[b] Shuhei Tamura,[b] Masahiro Kiyama,[b] Fumitaka Hayashi,[b] and Katsuya Teshima[a,b]†

In order to tailor the morphology of the layered double hydroxides (LDHs) particles, we focused on a synthesis method that involves the use of Al_2O_3 as a precursor, employing Al_2O_3 with different crystal structures (*e.g.*, α-Al_2O_3, ϑ-Al_2O_3, and γ-Al_2O_3) as well as amorphous Al_2O_3. When ϑ-Al_2O_3 and γ-Al_2O_3 were used, a three-dimensional network of plate-shaped LDH particles was formed even though α-Al_2O_3 barely reacts to form the LDH phase. Finally, adsorption tests involving HPO_4^{2-} ions confirmed that the fabricated LDH particles exhibited high ion-removal rates. Hydrogen phosphate ions (HPO_4^{2-}) in a concentration of 0.40 mmol g^{-1} could be removed completely within 10 min using the LDH particles prepared with ϑ-Al_2O_3 and γ-Al_2O_3; this is approximately 20 times shorter than the time taken by the LDH particle prepared from amorphous Al_2O_3.

Introduction

Layered double hydroxides (LDHs), which include hydrotalcite-like compounds and anionic clays, as attracting a lot of attention because of their ion-removal properties. These materials can be represented by the general formula $[M^{2+}_{1-x}M^{3+}_x(OH)_2]^{x+}[A_{nx/n}]^{x-}mH_2O$ and consist of octahedral brucite-like host layers (M^{2+}/M^{3+}: bivalent and trivalent metal cations), a charge-balancing anion (A^{n-}), and interlayer water molecules. Possible M^{2+} species include Mg^{2+}, Ni^{2+}, Zn^{2+}, and Ca^{2+}, among others, while possible M^{3+} species include Al^{3+}, Cr^{3+}, Fe^{3+}, and Co^{3+}, among others. The exchangeable anion, A^{n-}, can either be monovalent (*e.g.*, OH^-, F^-, Cl^-, or NO_3^-) or bivalent (*e.g.,* SO_4^{2-}, HPO_4^{2-} or CO_3^{2-}). LDHs are used in various applications and devices, such as ion-exchangers, catalysts, gas separators, and capacitors.[1-17] Their ion-exchange properties and, in particular, their selectivity and capacity, have been studied extensively by many researchers with respect to the removal of various combinations of metal cations. Miyata reported that the affinity of Mg-Al LDHs towards various anions can be arranged as follows: NO_3^- < Br^- < Cl^- < F^- < OH^- < MoO_4^{2-} < SO_4^{2-} < CrO_4^{2-} < $HAsO_3^{2-}$ <HPO_3^{2-} < CO_3^{2-}.[18] As can be seen from this list, bivalent oxo-anions such phosphate ions have a stronger affinity for Mg-Al LDHs.

However, even though Mg-Al LDHs exhibit strong attraction towards anions, their reaction rate during the ion-exchange reaction needs to be improved significantly if these materials are to find wider use. Recently, some effort to improve such ion-exchange properties have been carried out through various sophisticated synthesis routes for adsorbing methyl orange, methylene blue, and so on.[19-21] However, for example, Mg-Al LDHs take 4.0 h to remove nitrate ions when present in a concentration of 20.4 mg g^{-1}.[22] While activated biomaterials, which can remove nitrate ions in the same concentration in only 10 min.[22] In order to improve the reaction rate, the specific surface area of the LDH particles must be increased. Moreover, fabricating LDH materials with a high specific surface area in facile manner is important not only for improving their usability as ion-exchangers and catalysts but also from the viewpoint of material design. There have been several interesting developments in this regard. For instance, the synthesis of highly porous LDH particles[23] with a high specific surface area by a sol-gel-driven method has been reported recently. However, while these studies are important from a material design perspective, the processes involved are quite complex to be practical. Improving the dispersibility of LDH particles is important for ensuring a high specific surface area. However, the surface hydroxyl groups of LDHs are so inactive that it is difficult to modify their surface properties. Hence, in this study, we focused on the morphology control of LDH particles in order to improve the reaction rate.

It has been reported that LDH crystals can be formed using amorphous Al_2O_3 and MgO as precursors[24]. The generation of $Al(OH)_3$ on the surfaces of the Al_2O_3 particles, the subsequent diffusion of Mg^{2+} ions to the Al_2O_3 particles, and the ensuing reaction lead to the formation of stand-alone, hexagonal LDH particles. This suggests that the reactivity of the precursor may be exploited to vary the morphology of the fabricated LDH particles. Thus, we aimed to fabricate three-dimensional LDH particles by tuning the reactivity of Al_2O_3 and to improve the

[a] Research Initiative for Supra-Materials, Shinshu University, Japan Nagano 380-8553, Japan.
[b] Department of Materials Chemistry, Faculty of Engineering, Shinshu University, Nagano 380-8553, Japan.
† Contact address for the corresponding author: teshima@shinshu-u.ac.jp
Electronic Supplementary Information (ESI) available: SEM images and XRD patterns of Al_2O_3 precursors, FT-IR spectra of products formed during LDH synthesis, and cross-sectional SEM images and elemental maps of LDH particles prepared using ϑ-Al_2O_3 and γ-Al_2O_3 after HPO_4^{2-} ion adsorption tests (PDF). See DOI: 10.1039/x0xx00000x

rate of the reaction for removing anions, namely, phosphate ions, from water.

Experimental

Synthesis of LDH particles: The aluminum oxide particles used in this study as precursors included reagent-grade α-Al_2O_3 (Wako Pure Chemical Industries Ltd), ϑ-Al_2O_3 (Nippon Light Metal Company), γ-Al_2O_3 (Nippon Light Metal Company), and amorphous Al_2O_3, which was synthesized in the laboratory through the heat-decomposition of $Al(NO)_3 \cdot 9H_2O$ (Wako Pure Chemical Industries Ltd) at a holding temperature of 400 °C for 5 h. The method used for synthesizing the LDH particles was as follows. One of the aluminum oxide precursors was immersed in an aqueous solution containing MgO (Wako Pure Chemical Industries Ltd) in a Mg/Al ratio of 4:1 at 80 °C for about 120 h under atmospheric pressure. After 120 h holding, the precipitated powders were collected and filtered and then dried at 60 °C under atmospheric pressure.

Characterization of synthesized LDH particles: The structures of the obtained particles were studied by X-ray diffraction (XRD) analysis (Miniflex II, Rigaku), which was performed using a Cu-Kα radiation (λ = 0.154 nm) source operated at 30 kV and 20 mA. The scans were conducted for the 2ϑ range of 5 to 80°. The morphologies and sizes of the obtained particles were observed using field-emission scanning electron microscopy (FE-SEM, JSM-7400F, JEOL) at an accelerating voltage of 2–15 kV.

Energy-dispersive X-ray spectrometry (EDS, JSM-7000F, JEOL) was used to study the variation in the concentrations of the primary constituent elements on the surfaces and cross-sections of the synthesized LDH particles. Cross-sections of the particles were obtained using the focused ion-beam method (JIB-400, JEOL).

The specific surface areas of the LDH particles were calculated using the Brunauer–Emmett–Teller (BET) model based on the N_2 adsorption isotherms. The N_2 adsorption isotherms were measured at −196 °C using a Belsorp Mini II sorption analyzer (BEL, Japan). The LDH particles were degassed at 50 °C for 2 h prior to analysis.

The infrared (IR) spectra of the LDH particles were obtained using a Fourier transform infrared spectroscopy (FT-IR) system (FT/IR-6100, JASCO) with a smart-endurance single-bounce diamond attenuated total reflection cell (ATR PRO450-S, JASCO). The spectra for wavenumbers of 600 to 4000 cm^{-1} were obtained by adding 100 scans with a resolution of 4.0 cm^{-1}. Spectral manipulations, such as baseline correction, smoothing, and normalization, were performed using the Spectra Manager Ver.2 software package (JASCO).

Replacement of interlayer anionic species in LDH particles with Cl^- ions: Before the HPO_4^{2-} ion removal test, the interlayer anion species in the fabricated LDH particles were replaced with Cl^- ions. Reagent-grade HCl (Wako Pure Chemical Industries, Ltd.) and NaCl (Wako Pure Chemical Industries, Ltd.) were used for this purpose. The prepared LDH powders were immersed in an aqueous solution of 33 mM HCl and 4.0 M NaCl at room temperature and kept in this state overnight. This resulted in the interlayer anionic species being replaced by Cl^- ions.

Hydrogen phosphate ion (HPO_4^{2-}) adsorption tests: First, 1.0 g L^{-1} of the LDH particles was added to the test solution, which contained HPO_4^{2-} ions in a concentration of 100 ppm, in a glass beaker at 25°C. The solution was stirred using a cool stirrer (CSB-900S, AS ONE). The initial pH of the test solution was adjusted to 6.0 using diluted aqueous solutions of HCl and NaOH. Particles from the test solution were collected at 0, 10, 30, 60, 120, and 180 min and subjected to ion chromatography (HIS-20A SUPER, Shimazu; IonPac AS22 analytical column; IonPac AG22 guard column; and hydrogen carbonate/carbonate eluent) in order to evaluate the residual concentration of HPO_4^{2-} ions. The HPO_4^{2-} adsorption isotherm was analyzed using the following Langmuir model:

$$q_e = \frac{q_L b_L C_e}{1 + b_L C_e} \quad (1)$$

where q_e (mg g^{-1}) is the number of anions adsorbed at the equilibrium concentration, q_L is the maximum amount of the adsorbate adsorbed corresponding to the Langmuir model, b_L is the Langmuir constant, and C_e (mmol L^{-1}) is the equilibrium concentration. The experimental conditions were the same as mentioned above, except that the initial concentrations of HPO_4^{2-} ions were varied from 0.1 to 10 mM.

Results and discussion

Preparation and characterization of LDH particles: The effect of the polymorph of Al_2O_3 used as the precursor on the morphology of the synthesized LDH particles was investigated from the viewpoint of the reaction rate through XRD analysis. Figure 1 shows the XRD patterns of the powders collected from

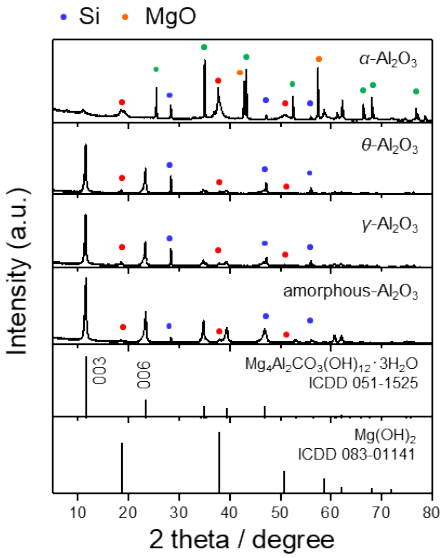

Fig. 1 XRD patterns of powders collected from reaction solution of Al_2O_3 precursor and MgO after 120 h (PDF 0511525, and PDF 08301141 were obtained from ICDD database); α-Al_2O_3, ϑ-Al_2O_3, γ-Al_2O_3, and amorphous Al_2O_3 were used as precursors.

the reaction solutions containing the various Al_2O_3 precursors and MgO after 120 h. It was confirmed that the LDH phase was

formed successfully when ϑ-Al_2O_3, γ-Al_2O_3, or amorphous Al_2O_3 was used, although a small amount of $Mg(OH)_2$ was also formed as a by-product. The high-intensity lines at approximately 11 and 22° can be attributed to the diffractions of the (003) and (006) planes of the LDH particles (ICDD PDF 083-01141). Further, when α-Al_2O_3 was used, the rate of the reaction between aluminum oxide and magnesium oxide was very low, resulting in the appearance of diffraction patterns related to the LDH particles as well as those related to α-Al_2O_3, MgO, and $Mg(OH)_2$. Further, the intensities of the LDH patterns were very low. These results were in keeping with those of the FT-IR measurements, which are shown in Figure S1. In the case of the powders obtained using ϑ-Al_2O_3, γ-Al_2O_3, and amorphous Al_2O_3, the IR spectra contained a peak related to the δ-mode of the O–H groups at approximately 600 cm^{-1}, in addition to a peak related to the strong ν_3 mode of CO_3^{2-} ions at 1380 cm^{-1} and a peak related to the weak ν_2 mode at 830 cm^{-1}. Peaks related to the water-bending mode were also observed in the lower-wavenumber region at approximately 1635–1650 cm^{-1}.[25-28] In the higher-wavenumber region, a high-intensity band centered at approximately 3400 cm^{-1} and attributable to the stretching modes of the hydroxyl groups in the LDH layers as well as the water molecules was observed.[25-28] These results also confirmed the successful formation of LDH particles. It should be noted that, in the case of the powders obtained using ϑ-Al_2O_3 and γ-Al_2O_3, $Mg(OH)_2$ was also present, as evidenced by the stretching peak observed at approximately 3700 cm^{-1}. The pH value of the reaction solution after 120 h was approximately 10 in all the cases. The precursor MgO turned into $Mg(OH)_2$ (brucite) in the aqueous solution; this was also true for all the cases. Similar trend could be shown in Raman spectra (please see Figure S2). The XRD diffraction patterns of the various Al_2O_3 precursors are shown in Figure S3. It can be seen that α-Al_2O_3 exhibits distinctly high crystallinity, while the other precursors have low crystallinity. The half width of the diffraction line of ϑ-Al_2O_3 was smaller than that of the γ-Al_2O_3 line, indicating that the crystallinity of ϑ-Al_2O_3 is higher than that of γ-Al_2O_3. This result suggests that the crystallinity, amount of defect and degree of distortion of crystal structure, of the Al_2O_3 precursor used might affects solid-state kinetics during formation of the LDH. The trend in the reactivity as observed from the XRD analysis was also confirmed from the SEM observations. In Figure 2, it can be seen that the powdered product prepared using α-Al_2O_3 consisted of aggregated, thin petal-shaped particles. The LDH particles formed using ϑ-Al_2O_3 and γ-Al_2O_3 consisted of thin, interconnected plate-like particles and tightly aggregated plate-like particles, respectively. An interesting point to note here is that the LDH particles produced using ϑ-Al_2O_3 were thicker. On the other hand, the LDH particles formed using amorphous Al_2O_3 consisted of aggregates of freestanding, plate-shaped particles. The SEM images of the respective precursors are shown in Figure S4. It can be seen that α-Al_2O_3 consisted of spherical particles with a diameter of 1.0 μm, while ϑ-Al_2O_3 and γ-Al_2O_3 consisted of aggregates of small particles with a diameter of about 500 nm and amorphous Al_2O_3 consisted of amorphous aggregates. At pH > 10, the precursor MgO turns into $Mg(OH)_2$, which then dissociates into Mg^{2+} and

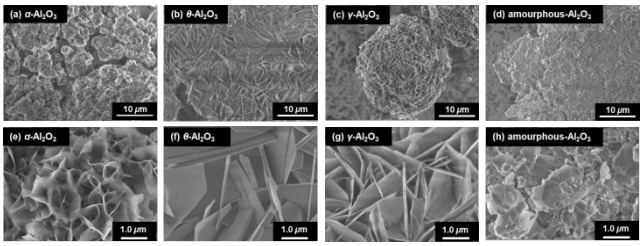

Fig. 2 FE-SEM images of powders collected from reaction solution containing Al_2O_3 precursor and MgO after 120 h in case of (a, e) α-Al_2O_3, (b, f) ϑ-Al_2O_3, (c, g) γ-Al_2O_3, and (d, h) amorphous Al_2O_3.

OH^- ions. Given this fact, we propose the following manner for the formation of the LDH. During synthesis using α-Al_2O_3, the Al_2O_3 particles get aggregated, and their surface morphology changes, with the particles becoming petal-like owing to the formation of the LDH particles and $Mg(OH)_2$ on the surfaces of the Al_2O_3 particles. During synthesis using ϑ-Al_2O_3 and γ-Al_2O_3, the reaction of the precursor aggregates with Mg^{2+} and OH^- ions commences on the surfaces of the Al_2O_3 particles, leading to the formation of plate-shaped particles. Finally, during synthesis using amorphous Al_2O_3, the Al_2O_3 dissolves readily and reacts with Mg^{2+} ions to form stand-alone LDH particles.

In order to confirm this hypothesis, cross-sectional SEM images of the particles of the LDH particles prepared using ϑ-Al_2O_3 and γ-Al_2O_3 and elemental maps showing the contents of oxygen, magnesium, and aluminum in the particles were obtained (see Figure 3). In the case of the particles produced using ϑ-Al_2O_3 as the precursor, plate-shaped particles were observed inside the whole area of LDHs particles. Moreover, elemental mapping indicated that magnesium and aluminum elements were distributed all over the LDH particles. In the case of the LDH particle prepared using γ-Al_2O_3, most of the particles were plate-shaped and had formed aggregates. It is worth noting that a few spherical particles were also present (see Figure S5); in the case of these particles, an aluminum-rich region was present at the center, and the particles themselves were surrounded by the plate-shaped particles, with a large void present between them. This geometric feature indicated that Al_2O_3 had acted as the core and that the dissolution rate of Al_2O_3 was higher than the diffusion rate of Mg^{2+} ions, that is had occurred, resulting in the formation of the LDH particles. This clearly confirms that the reactivity of the Al_2O_3 precursor used (the reactivity of γ-Al_2O_3 is higher than that of ϑ-Al_2O_3) has a

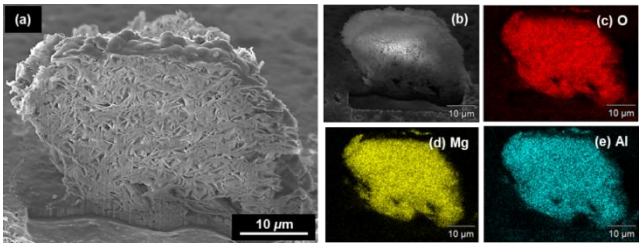

Fig. 3 (a) A cross-sectional SEM image and (b-e) elemental maps of LDH particles prepared using ϑ-Al_2O_3.

determining effect on the morphological features of the resulting LDH particles.

The results of the BET analysis indicated that the specific surface areas of the LDH particles prepared using ϑ-Al_2O_3 and γ-Al_2O_3 were high at 33.5 and 24.4 $m^2\ g^{-1}$, respectively, while that of the LDH particles prepared using amorphous Al_2O_3 was 15.3 $m^2\ g^{-1}$. Which is reflected by the pore-size distribution (in Figure S6) that shows the LDH particles prepared using ϑ-Al_2O_3 and γ-Al_2O_3 have various pore-size, although the one prepared using amorphous Al_2O_3 have a quite small distribution.

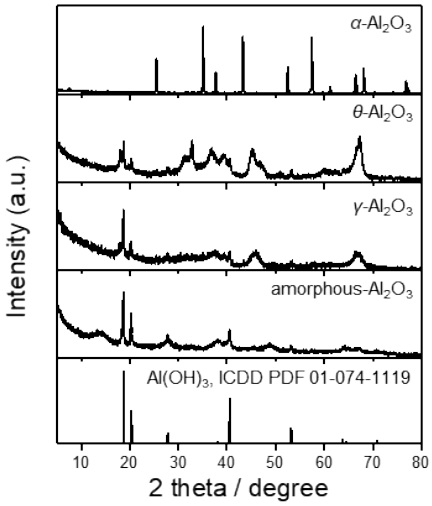

Fig. 4 XRD patterns of powders collected from reaction solution containing Al_2O_3 precursor after 120 h (PDF 01-074-1119 was obtained from ICDD database); α-Al_2O_3, ϑ-Al_2O_3, γ-Al_2O_3, and amorphous Al_2O_3 were used as precursors.

There results strongly suggested that the reactivity of the Al_2O_3 precursor affects the reaction rate and hence the morphology of the LDH particles formed. Thus, a simple verification test to determine the reactivities of the various Al_2O_3 precursors were performed. Powders of the Al_2O_3 precursors were immersed in an aqueous solution at 80 °C for 48 h in the absence of MgO, and the mixtures were subjected to XRD analysis in order to analyze the differences in their crystal structures (Figure 4). Although the chemical structure of α-Al_2O_3 barely changed, both ϑ-Al_2O_3 and γ-Al_2O_3 partially transformed into $Al(OH)_3$, while all of the amorphous Al_2O_3 was converted into $Al(OH)_3$. These results confirm that the reactivities of the various Al_2O_3 precursors can be arranged in the following decreasing order: α-Al_2O_3, ϑ-Al_2O_3, γ-Al_2O_3, and amorphous Al_2O_3. At the same time, they also suggest that the synthesis route employed in this study involves the transformation of Al_2O_3 into $Al(OH)_3$, which then reacts with Mg^{2+} and OH^- ions to form the LDH. The reactivity of Al_2O_3 is determined by the coordination structure around the Al atoms. This coordination structure is described in Figure 5. In the case of α-Al_2O_3, the Al atoms coordinate with six O atoms, and the octahedral unit connects to the neighboring one in an edge-sharing manner. On the other hand, in ϑ-Al_2O_3, the Al atoms coordinate with four and/or six O atoms, and the tetrahedral unit connects to an octahedral unit in a corner-sharing manner, while two octahedral units connect to each other in an edge-sharing manner. Finally, in γ-Al_2O_3, the octahedral units connect to each other in an edge-sharing manner as well as to the tetragonal unit in a face-sharing manner. Thus, many vacancies exist at the Al sites. The existence of the above-mentioned edge-sharing part and vacancies significantly affect the reactivity of Al_2O_3 with water to form $Al(OH)_3$. It should be noted that, between ϑ-Al_2O_3 and γ-Al_2O_3, the former exhibits a lower reactivity and that the rate of the reaction for the dissolution of Al_2O_3 to form $Al(OH)_3$ is equal to that of the reaction for LDH formation, resulting in a homogeneous elemental distribution and hence homogenous geometry, as shown in Figure 3. In addition, the LDH particles produced with ϑ-Al_2O_3 consisted of thicker, more erect plate-shaped particles. This might be because of the differences in the crystal structures of the precursors used. Among ϑ-Al_2O_3, γ-Al_2O_3, and α-Al_2O_3, whose crystal structures all consist of edge-sharing octahedral units, ϑ-Al_2O_3 has a structure similar to that of the intermediate $Al(OH)_3$. This suggests that the formation of thicker, more erect LDH particles in the case of ϑ-Al_2O_3 can probably be attributed to an uninterrupted topotactic-like reaction, as indicated in Figure 5. To summarize, in light of the differences in the reactivities of the Al_2O_3 polymorphs used and the topotactic route employed in this study, the crystal structure of the Al_2O_3 precursor used and, in particular, its similarity to that of the reaction intermediate $Al(OH)_3$, has a determining effect on the rate of dissolution of the Al_2O_3 core and hence the thickness and three-dimensional architecture of the resulting LDH particles.

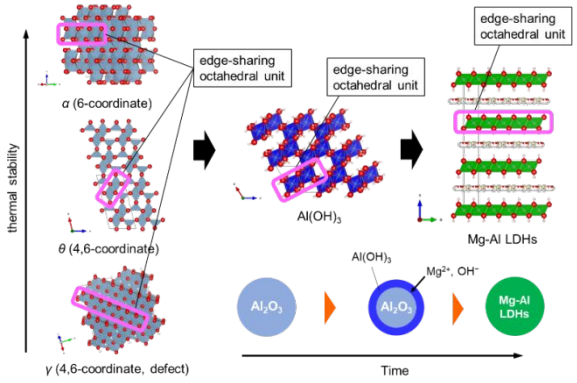

Fig. 5 Formation manners of LDH powders using various Al_2O_3 precursors.

Hydrogen phosphate ion (HPO_4^{2-}) adsorption tests: Adsorption tests of HPO_4^{2-} ions were performed using the LDH particles prepared with ϑ-Al_2O_3, γ-Al_2O_3, and amorphous Al_2O_3 after they had been subjected to a pretreatment to replace their interlayer anionic species with Cl^- ions. Figure S7 shows the XRD pattern of the above-mentioned LDHs before and after the treatment, where the slight shift of 003 diffraction line to lower 2ϑ value was observed in all LDHs. This implies successful replacement with Cl^- ions. Figure 6 shows the time dependence of the amount of HPO_4^{2-} ions adsorbed. The LDH particles produced using ϑ-Al_2O_3 and γ-Al_2O_3 exhibited relatively rapid

ion-removal rates and could remove all the HPO_4^{2-} ions present in a concentration of 0.40 mmol g^{-1} within 10 min, while the LDH particles prepared using amorphous Al_2O_3 took 3.0 h for to remove the same amount of HPO_4^{2-} ions. The difference in the concentrations in which HPO_4^{2-} ions were removed by the ϑ-Al_2O_3 and γ-Al_2O_3 LDH particles (0.41 and 0.45 mmol g^{-1}, respectively) was very small. However, this small difference is probably attributable to the difference in the morphological characteristics of the LDH particles. Finally, to elucidate how these factors affect the adsorption sites, an equilibrium adsorption isotherm was analyzed. Figure S8 shows the adsorption isotherms for HPO_4^{2-} ions, which indicates the good fit to the Langmuir model regarding as the above-mentioned three samples. The Langmuir model assumes that all the adsorption sites are equivalent and homogeneous to form a monolayer of adsorbates, and at the same time the adsorption energy is independent of whether the ion-exchange sites are occupied or not. Therefore, we concluded that the LDH particles prepared in this study possess homogeneous adsorption sites in their crystal structure in addition to unique three-dimensional morphology.

Next, cross-sectional imaging and elemental mapping were performed on the LDH particles after the HPO_4^{2-} ion adsorption test for 120 h in order to determine their phosphorous, magnesium, and aluminum contents. Figure S9 shows that

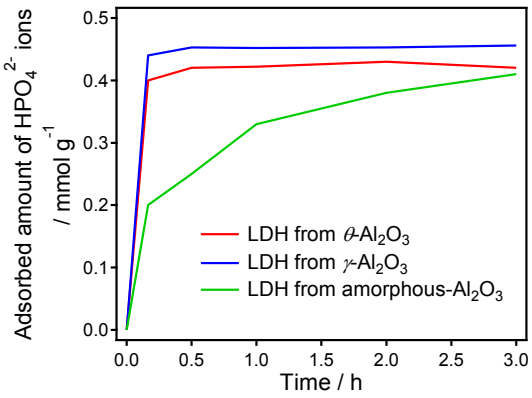

Fig. 6 The dependence of adsorbed amount of HPO_4^{2-} ions in test solution on testing time during ion-removal tests performed using LDH particles prepared with ϑ-Al_2O_3, γ-Al_2O_3, and amorphous Al_2O_3.

phosphorous atoms were distributed all over the LDH particles in the case of the particles produced using ϑ-Al_2O_3 and γ-Al_2O_3. This indicates that, during the adsorption of HPO_4^{2-} ions, the ions infiltrate the three-dimensional LDH particles. Thus, the three-dimensional architecture of the particles, which is controlled by the reactivity of the Al_2O_3 precursor used, effectively improves the reaction rate of anion removal. In our future works, we hope to study the architecture of LDHs in greater detail, for example, using Al_2O_3 with a more complex particle morphology, with the aim of designing and synthesizing LDHs better suited for use in ion adsorption, catalyst reactions, and gas separation, among other applications.

Conclusions

Mg-Al LDH particles with a three-dimensional architecture were successfully fabricated using Al_2O_3 precursors with different reactivities, namely, α-Al_2O_3, ϑ-Al_2O_3, γ-Al_2O_3, and amorphous Al_2O_3. Only when ϑ-Al_2O_3 and γ-Al_2O_3, which exhibit moderately high reactivities, were used as the precursor, was as three-dimensional network of plate-shaped LDH particles formed. On the other hand, the use of α-Al_2O_3, which has the lowest reactivity, barely resulted in an LDH phase while amorphous Al_2O_3, which has the highest reactivity, resulted in aggregates of particles. The crystal structure of the Al_2O_3 precursor used and, in particular, its similarity to that of the reaction intermediate $Al(OH)_3$, probably has a determining effect, in light of its reactivity and the topotactic-like route used in this study, on the reaction rate of the dissolution of the Al_2O_3 core and hence the thickness and three-dimensional architecture of the formed LDH particles. The results of a BET analysis also indicated that the specific surface area of the LDH particles prepared using ϑ-Al_2O_3 and γ-Al_2O_3 were higher (33.5 and 24.37 m^2 g^{-1}, respectively) than that of the particles prepared using amorphous Al_2O_3 (15.34 m^2 g^{-1}). Finally, adsorption tests involving HPO_4^{2-} ions showed that the former exhibited superior ion-removal rates and could remove HPO_4^{2-} ions in a concentration of 0.40 mmol g^{-1} within 10 min, which is approximately 20 times faster than the LDH particle prepared from amorphous Al_2O_3. These results show conclusively that the three-dimensional architecture of the fabricated LDH, which is controlled by the reactivity of the Al_2O_3 precursor used, effectively improves the reaction rate for anion removal from water.

Acknowledgements

This work was partly supported by the following four national grants. (1) Japan Society for the Promotion of Science (JSPS) Grant-in-Aid for Scientific Research (A) 25249089, (2) the "A Shinshu-Method for Regional Innovation Ecosystem by Industrial Implementation of Innovative Inorganic Crystal Material Technology" project of the "Program on Regional Innovation and Ecosystem Formation" of the Ministry of Education, Culture, Sports, Science and Technology (MEXT), Japan, (3) the Matching Planner Program of the Japan Science and Technology Agency (JST), and (4) the Environment Research and Technology Development Fund 5RF-1902 of the Environmental Restoration and Conservation Agency of Japan.

Notes and references

1 H. Fan, J. Zhu, J. Sun, S. Zhang and S. Ai, *Chem. - A Eur. J.*, 2013, **19**, 2523–2530.
2 F. Leroux and J. Besse, *Chem. Mater.*, 2001, **13**, 3507–3515.
3 L. Li, Y. Feng, Y. Li, W. Zhao and J. Shi, *Angew. Chemie - Int. Ed.*, 2009, **48**, 5888–5892.
4 G. Abellán, C. Martí-Gastaldo, A. Ribera and E. Coronado, *Acc. Chem. Res.*, 2015, **48**, 1601–1611.
5 M. S. Yarger, E. M. P. Steinmiller and K. S. Choi, *Inorg. Chem.*, 2008, **47**, 5859–5865.

6 M. Shao, F. Ning, M. Wei, D. G. Evans and X. Duan, *Adv. Funct. Mater.*, 2014, **24**, 580–586.
7 Y. Zhao, Y. Zhao, G. I. N. Waterhouse, L. Zheng, X. Cao, F. Teng, L. Z. Wu, C. H. Tung, D. O'Hare and T. Zhang, *Adv. Mater.*, , DOI:10.1002/adma.201703828.
8 D. P. Debecker, E. M. Gaigneaux and G. Busca, *Chem. - A Eur. J.*, 2009, **15**, 3920–3935.
9 P. Sahoo, S. Ishihara, K. Yamada, K. Deguchi, S. Ohki, M. Tansho, T. Shimizu, N. Eisaku, R. Sasai, J. Labuta, D. Ishikawa, J. P. Hill, K. Ariga, B. P. Bastakoti, Y. Yamauchi and N. Iyi, *ACS Appl. Mater. Interfaces*, 2014, **6**, 18352–18359.
10 L. Ma, S. M. Islam, C. Xiao, J. Zhao, H. Liu, M. Yuan, G. Sun, H. Li, S. Ma and M. G. Kanatzidis, *J. Am. Chem. Soc.*, 2017, **139**, 12745–12757.
11 B. M. Hunter, W. Hieringer, J. R. Winkler, H. B. Gray and A. M. Müller, *Energy Environ. Sci.*, 2016, **9**, 1734–1743.
12 S. Tezuka, R. Chitrakar, A. Sonoda, K. Ooi and T. Tomida, *Chem. Lett.*, 2003, **32**, 722–723.
13 J. Das, B. S. Patra, N. Baliarsingh and K. M. Parida, *Appl. Clay Sci.*, 2006, **32**, 252–260.
14 D. Ivánová, P. Albert and J. Kavuličová, *Appl. Clay Sci.*, 2018, **152**, 65–72.
15 R. Sasai, W. Norimatsu and Y. Matsumoto, *J. Hazard. Mater.*, 2012, **215**–**216**, 311–314.
16 S. Tezuka, R. Chitrakar, A. Sonoda, K. Ooi and T. Tomida, *Adsorption*, 2005, **11**, 751–755.
17 Q. Wang and D. O'Hare, *Chem. Rev.*, 2012, **112**, 4124–4155.
18 S. Miyata, *Clays Clay Miner.*, 1983, **31**, 305–311.
19 Y. Chen, C. Jing, X. Zhang, D. Jiang, X. Liu, B. Dong, L. Feng, Y. Zhang, *J. Colloid. Interf. Sci.* 2019, **548**, 100–109.
20 D. BinJiang, C. Jing, Y. Yuan, L. Feng, X. Liu, F. Dong, B. Dong, Y. Zhang, *J. Colloid. Interf. Sci.* 2019, **540**, 398–409.
21 S.K. Dutta, S. Chakraborty, *Ind. Eng. Chem. Res.* 2019, **58**, 11985−11998.
22 A. Bhatnagar, M. A. Sillanpää, *Chem. Eng. J.* 2011, **168**, 493–504.
23 Y. Tokudome, T. Morimoto, N. Tarutani, P. D. Vaz, C. D. Nunes, V. Prevot, G. B. G. Stenning and M. Takahashi, *ACS Nano*, 2016, **10**, 5550–5559.
24 Z.P. Xu, G. Q. Lu, *Chem. Mater.*2005, **175**, 1055-1062.
25 Z.P. Xu, H.C. Zeng, *J. Phys. Chem. B* **2001**, *105*, 1743–1749.
26 C. J. Serna, J.L. Rendon, J.E. Iglesias, *Clays Clay Miner.* **1982**, *30*, 180–184.
27 J.T. Kloprogge, L. Hickey, R.L. Frost, *J. Raman Spectrosc.* **2004**, *35*, 967–974.
28 J.T. Kloprogge, L.Hickey, R. L. Frost, *Am. Mineral.* **2002**, *87* 623–629.

